Probabilistic conversion of neurosurgical DBS electrode coordinates into MNI space

Andreas Horn[1,2*], Andrea A. Kühn[2], Angela Merkl[2], Ludy Shih[2], Ron Alterman[1,3] and Michael Fox[1]

1 Berenson-Allen Center for Noninvasive Brain Stimulation, Department of Neurology, Beth Israel Deaconess Medical Center, Harvard Medical School, Boston, MA 02215

2 Charité – University Medicine Berlin, Department of Neurology, Movement Disorder and Neuromodulation Unit

3 Beth Israel Deaconess Medical Center, Neurosurgery Department, Harvard Medical School, Boston, MA 02215

***** Corresponding author:

Dr. Andreas Horn
Berenson-Allen Center for Noninvasive Brain Stimulation
Department of Neurology, Beth Israel Deaconess Medical Center
Harvard Medical School
330 Brookline Ave
Boston, MA 02215
E-Mail: ahorn1@bidmc.harvard.edu
Phone: +1 6174077649

Abstract

In neurosurgical literature, findings such as deep brain stimulation (DBS) electrode positions are conventionally reported in relation to the anterior and posterior commissures of the individual patient (AC/PC coordinates). However, the neuroimaging literature including neuroanatomical atlases, activation patterns, and brain connectivity maps has converged on a different population-based standard (MNI coordinates). Ideally, one could relate these two literatures by directly transforming MRIs from neurosurgical patients into MNI space. However obtaining these patient MRIs can prove difficult or impossible, especially for older studies or those with hundreds of patients. Here, we introduce a methodology for mapping an AC/PC coordinate (such as a DBS electrode position) to MNI space without the need for MRI scans from the patients themselves. We validate our approach using a cohort of DBS patients in which MRIs are available, and test whether several variations on our approach provide added benefit. We then use our approach to convert previously reported DBS electrode coordinates from eight different neurological and psychiatric diseases into MNI space. Finally, we demonstrate the value of such a conversion using the DBS target for essential tremor as an example, relating the site of the active DBS contact to different MNI atlases as well as anatomical and functional connectomes in MNI space.

Introduction

In the field of functional neurosurgery, target locations have been described using coordinates of a defined stereotactic space since 1906 (Clarke and Horsley, 1906). Currently, the Schaltenbrand-Wahren atlas for stereotaxy of the human brain (Schaltenbrand et al., 1977) and the Talairach Co-planar stereotactic Atlas of the Human Brain (Talairach and Tournoux, 1988) serve as standards for reporting brain locations with respect to the anterior commissure (AC) and posterior commissure (PC). Both the AC and PC are small structures that can clearly be identified and are considered relatively invariant in their spatial location (Brett et al., 2002). The largest studies of deep brain stimulation (DBS) for a variety of neurological and psychiatric indications have reported electrode locations in ACPC coordinates (Table 1). In contrast to neurosurgery, the neuroimaging field has gradually moved away from the single-subject AC/PC standard to population-based atlases. In 1994, the Montreal Neurological Institute (MNI) matched anatomical images of 305 subjects to the Talairach brain (Collins, 1994), which was iteratively refined to the MNI152 2009 NLIN atlas (Fonov et al., 2009). This MNI atlas space has become the standard for reporting results across thousands of neuroimaging studies.

Given these different coordinate system standards, it is difficult to relate findings in the neurosurgical literature (such as clinical DBS response at a given AC/PC coordinate) to findings in the neuroimaging literature (such as activation or connectivity). Relating these two atlas standards is potentially valuable as there are an increasing number of resources available in MNI space that could lend insight into the effect of stimulation at a given brain location (Fox et al., 2014; Horn and Kühn, 2015; Höflich et al., 2010). These MNI resources include subcortical atlases based on histology (Amunts et al., 2013; Chakravarty et al., 2006; Jakab et al., 2012; Krauth et al., 2010; Morel, 2013; Yelnik et al., 2007), high-

field MRI (Keuken et al., 2013; 2014), structural connectivity (Accolla et al., 2014; Behrens et al., 2003) and functional connectivity (Choi et al., 2012; Zhang et al. 2008). Beyond atlases, there are increasingly detailed structural and functional connectome datasets in MNI space (Horn, 2015; Mori et al., 2008; Yeh and Tseng, 2011; Yeo et al., 2011; Setsompop et al., 2013; van Essen et al., 2012) that can be used to investigate the connectivity properties of DBS targets (Fox et al., 2014) or brain lesions (Boes et al., 2015; Laganiere et al., 2016; Fischer et al., 2016; Darby et al., 2016).

There are several potential options for converting AC/PC coordinates from a neurosurgical study into MNI space. By far the best option is to obtain the MRI data from the neurosurgical patients included in the study and directly warp their brains into MNI space. This allows for direct conversion between each patient's AC/PC coordinates and MNI coordinates. Indeed some neurosurgical studies are beginning to use this approach and report results in MNI space (Barow et al., 2014; Hohlefeld et al., 2015; Horn and Kühn, 2015; Merkl et al., 2015; 2013; Neumann et al., 2015a; 2015b; Riva-Posse et al., 2014; Schönecker et al., 2009; Schroll et al., 2015). However, these studies are few relative to the wealth of information in the neurosurigical literature. For example, papers reporting MNI coordinates of DBS sites for Parkinson's disease range from 10-20 patients (e.g. Barow et al., 2014; Neumann et al., 2015), compared to >150 patients for papers reporting AC/PC coordinates (e.g. Caire et al., 2013). Moreover, for most treatment indications, no studies have reported MNI coordinates (Höflich et al., 2010; see Table 1). Obtaining pre and post operative neuroimaging from all these neurosurgical cohorts for direct transformation into MNI space is difficult if not impossible. A conversion tool between AC/PC coordinates and MNI space that does not require the original MRI scans from the neurosurgical patients themselves would be valuable.

However, transforming between coordinate systems is not straightforward. For example, the MNI brain is substantially larger than average (Allen et al., 2002), whereas the Talairach brain is smaller than average (Figure 1). Talairach-to-MNI conversion tools based on linear (Brett et al., 2002; Lancaster et al., 2007) and nonlinear transforms (Lacadie et al., 2008) were designed to map from *Talairach* to MNI – not from AC/PC coordinates used in functional surgery. Explicitly, surgical coordinates are often reported relative to the patient's midcommisural point (MCP) or even the PC, requiring an initial conversion into AC-based Talairach-coordinates. This additional conversion step requires knowing the AC-PC distance of the cohort, which is rarely reported (for exceptions see Papavassiliou et al., 2004; Ponce et al., 2015). The AC-PC distance varies between Talairach and MNI space, from 19 to 32 mm across single subjects, and from 24.9 to 28.3 mm across different populations (Figure 1; Fiandaca et al., 2011; Lee et al., 2008; Liang et al., 2015; Papavassiliou et al., 2004). Moreover, the exact landmarks used to define the AC and PC themselves vary across centers (Weiss et al., 2003; Figure 1 b).

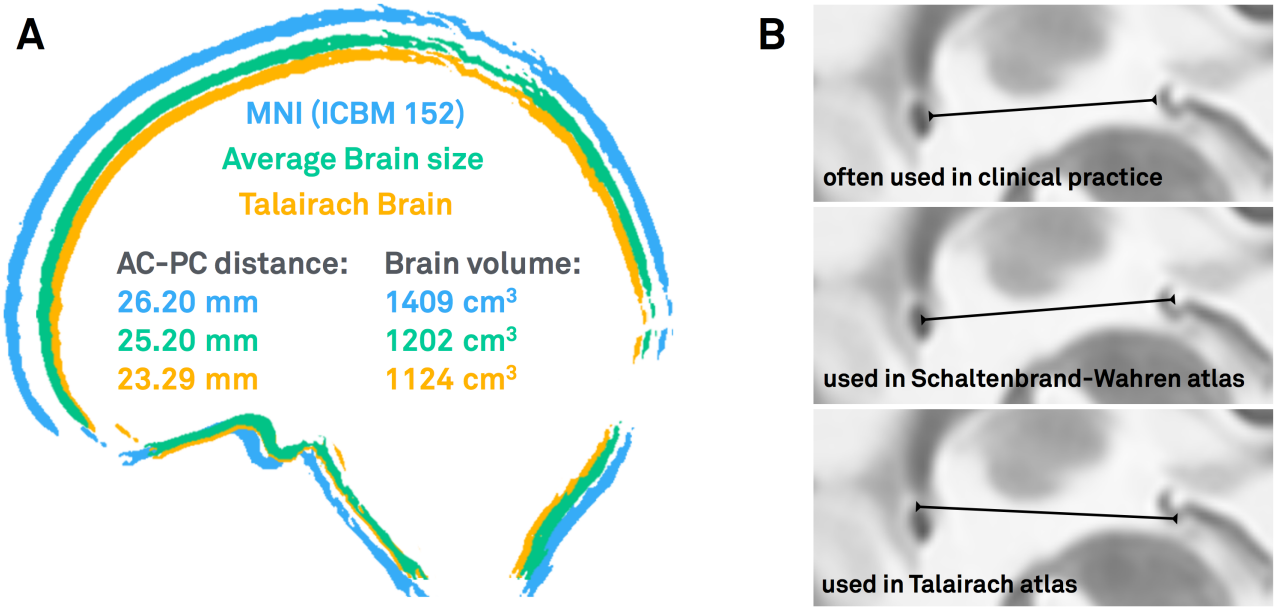

Figure 1 a) Schematic illustrating differences in size of an average brain, the MNI brain and the Talairach brain (data from Allen et al., 2002; Lee et al., 2008). b) Different ways to measure AC/PC distance and place fiducials for the AC-PC line (see Weiss et al., 2003).

The upper case was used in this study, the other two used in reference atlases often used in neurosurgical literature (Schaltenbrand et al., 1977; Talairach et al., 1988).

Here, we present a method that converts AC/PC coordinates to MNI space in a probabilistic fashion. In contrast to the solutions mentioned above, mappings are carried out using the individual anatomy in large cohorts of subjects. We validated our approach using two cohorts of DBS patients, one with Parkinson's disease (PD) with DBS to the subthalamic nucleus (STN) and one with Treatment-resistant Depression (TRD) with DBS to the subcallosal cingulate (SCC; Merkl et al., 2015). We chose the PD cohort because the STN is the most common stereotactic target world-wide and spatially close to the AC and PC. We chose the TRD cohort because the subcallosal cingulate is much further from the AC-PC line, helping test for generalizability of our approach. Following validation, we then use our approach to transform average AC/PC coordinates reported in the neurosurgical DBS literature into MNI space. Finally, we demonstrate how using such a conversion allows one to take advantage of MNI-based atlases and tools such as anatomical and functional connectomes to better characterize DBS locations.

Methods

Subject cohorts and imaging

450 subjects total from five cohorts were used in this study. The reason for including different cohorts was to determine the relative value of using young healthy subjects, age-matched, disease-matched, or disease severity matched cohorts for our probabilistic mapping.

1. *Young*: 32 young healthy subjects were downloaded from the Human Connectome Project database (mean age 31.5 years ± 8.6 SD, 14 female, see acknowledgements; Setsompop et al., 2013). 3 subjects of the original 35 were excluded because they lacked a T2-weighted anatomical image. T2-weighted images had an isotropic voxel size of 0.7 mm and were acquired on the customized MGH Siemens 3T Connectome scanner. Detailed scanning parameters can be found on the project website (https://ida.loni.usc.edu/).

2. *PD DBS Patients*: 39 PD patients were treated with DBS to the STN (mean age 59.0 years ± 7.9 SD, 14 female). Details regarding this patient cohort are available in supplementary material (S1). T2-weighted images had an in-plane axial resolution of 0.51 × 0.51 mm and a slice thickness of 2 mm. Detailed scanning parameters have been published previously (Horn and Kühn, 2015). Patients in this cohort are referred to as *other DBS patients* when comparing single mappings of one patient to the mapping based on the rest of the group (leave-one-out design).

3. *PD Disease Matched*: 160 PD patients were downloaded from the from the Parkinson's progression markers initiative (PPMI) database PPMI database (mean age 61.3 ± 9.4 SD, 56 female). T2-weighted images had an in plane resolution of

0.94 × 0.94 and a slice thickness of 3 mm. Detailed scanning parameters can be found on the project website (www.ppmi-info.org).

4. *TRD DBS Patients*: 9 patients suffering from treatment-resistant depression (TRD) underwent DBS surgery to the subcallosal cingulate (mean age: 50.11 years ± 12.73 SD, 4 women). Details regarding this patient cohort have been published previously (Merkl et al., 2015). T2-weighted images had an in-plane axial resolution of 0.51 × 0.51 mm and a slice thickness of 2 mm. Detailed scanning parameters have been published previously (Horn and Kühn, 2015). As above, patients in this cohort are referred to as *other DBS patients* when comparing single mappings of one patient to the mapping based on the rest of the group (leave-one-out design).

5. *Age matched*: 564 healthy subjects with a large age range (mean age: 48.12 years ± 16.5 SD, age range 19-86 years, 341 women) were downloaded from the IXI database (http://brain-development.org/ixi-dataset/; Kuklisova-Murgasova et al., 2011). T2-weighted images had a resolution of 0.94 × 0.94 × 1.00 mm. Detailed scanning parameters can be found on the project website. For each AC/PC coordinate from a DBS study, 30 subjects of the 564 were chosen to match the mean age of the DBS patient population. In total, 210 subjects from this dataset were used in the present analysis.

Identifying the AC and PC

In the neurosurgical literature, AC and PC are usually marked manually and the MCP is computed. However this process is a known source of error (Pallavaram et al., 2015; 2008) and would be labor intensive for the 450 subjects in the current analysis. We therefore used a transform to automatically place fiducials of AC, PC and a mid-sagittal point (MSP) within each subject's native space. Literature results suggest that this process

is feasible and even favorable compared manual AC/PC mapping (Pallavaram et al., 2015). Still, to confirm this on our data, the AC and PC were manually marked using axial and sagittal views on all subjects of the *Young* and the *DBS patients (PD)* cohorts using 3D Slicer 4.5 (www.slicer.org) by a trained expert. The same fiducials were additionally marked on the ICBM 2009b nonlinear T2-weighted MNI template. The latter were transformed from MNI into native space using Advanced Normalization Tools (ANTs) SyN registration (Avants et al., 2008) as implemented in Lead-DBS and compared to their manually marked counterparts by computing RMS distance errors and Pearson's correlation coefficients of x-, y- and z-coordinates independently.

Converting DBS electrode coordinates in AC/PC space to MNI

In the *PD DBS and TRD DBS patient* cohorts, electrode contacts could be manually localized in native as well as in MNI space. Thus, these imaging data served as a gold-standard of AC/PC to MNI conversions. Electrode contacts were localized in native space with respect to the MCP (AC/PC coordinates), as per convention in the neurosurgical literature (Weiss et al., 2003). The coordinates of the electrode contact active >12 months after surgery was recorded. Preoperative and postoperative MRIs from each DBS patient were then co-registered and normalized into MNI space using the nonlinear SyN approach as implemented in ANTs/Lead-DBS. The location of the same contact was then directly identified in MNI space as described in (Horn and Kühn, 2015).

Because MRIs from the patients themselves are often unavailable, for example when an AC/PC coordinate comes from the neurosurgical literature, we tested several other approaches for converting AC/PC coordinates to MNI space. The results of each approach were then compared to the gold standard as described above. The first and simplest approach, referred to as *MNI survey*, involved defining the AC, PC, and MCP on the MNI template brain (ICBM 2009b nonlinear T2 asymmetric) then marking a point at the same x,

y, and z distances as measured in the patient's brain. The second approach involved converting AC/PC coordinates measured in each patient (defined relative to the MCP) into Talairach coordinates (defined relative to the AC), then transforming these Talairach coordinates to MNI space using either the TAL2MNI (Brett et al., 2002) or TAL2ICBM (Lancaster et al., 2007) transforms. To convert MCP to AC coordinates, we added ½ the average AC/PC distance to the y coordinate. A value of 25.64 mm was used for the average AC/PC distance, derived from a large cohort of 60-69 year old caucasians (Lee et al., 2008).

Note that both the MNI survey and the Talairach to MNI transforms define just a single point in MNI space. However without the patient's own MRI, the exact location of a given AC/PC coordinate in MNI space is unknown and may be better represented as a probabilistic distribution. To create such a distribution, we mapped each AC/PC coordinate to a group of individual subjects in native space, then used a nonlinear warp to determine where that AC/PC coordinate would appear in MNI space. Because individual subjects differ in their anatomy and AC-PC distances, a single point in AC/PC space will be represented as a three-dimensional point cloud in MNI space. The average coordinates from this point cloud represent the center of this distribution (as reported in table 1) and all statistics such as whether the point cloud spreads more in one direction than another were performed on this distribution. However, for visualization purposes, we found it helpful to convert the point cloud to a Gaussian distribution. A 3D Gaussian distribution was fitted to the points using Matlab 2015b (the Mathworks, Natick, MA). This allows us to color code the distribution so the center and spread can be easily visualized. Gaussian distributions were visualized using Lead-DBS software (figs. 3&4). Different groups of subjects could conceivably be used for this probabilistic conversion. For the PD-DBS patients, we tested the accuracy of our probabilistic transform using a young cohort, age-matched cohort, disease-matched cohort, and disease severity-matched cohort (other PD DBS patients).

Probabilistic transforms for the TRD-DBS patients were tested using the young cohort, age-matched cohort, and a disease-severity matched cohort (other TRD DBS patients). Mappings were compared to the gold standard and resulting errors were compared between methods using a one-way ANOVA analysis pairwise multiple comparison post-hoc tests between each pair of approaches using Tukey's Honest Significant Difference procedure. Variance of probabilistic mappings along x-, y- and z-axes was compared using Bartlett‘s test and F-tests for post-hoc head-to-head comparisons.

Calculation of MNI coordinates for standard DBS targets based on literature findings

AC/PC coordinates of effective DBS contacts defined relative to the MCP were retrieved via literature research for the most common DBS targets. Our list of diseases and DBS targets was largely informed by (Lozano and Lipsman, 2013). However five of eleven diseases were excluded due to lack of human experiments (tinnitus, schizophrenia), target heterogeneity (epilepsy, chronic pain), or target overlap with another disease (anorexia nervosa matches the target used in treatment-refractory major depression). For a detailed description of how DBS targets were selected from literature results for each disease, see supplementary material (S2). Each AC/PC coordinate was converted into MNI space using the above probabilistic mapping approach and a set of age-matched MRIs. X-, y- and z-coordinates of single warps were tested to conform to a Gaussian distribution using the Chi-square goodness-of-fit test. The Gaussian fit illustrated in figs. 2-4 was performed by calculating mu and Sigma from the samples.

MNI resources and connectivity mapping from probabilistic DBS targets

To demonstrate why converting a DBS target previously reported in AC/PC coordinates into MNI space might be useful, we used the DBS target for essential tremor as an

example. Thalamic atlases in MNI space were identified via a literature and web search. Some of these atlases needed an additional warp into ICBM 2009b nonlinear space used in this study. For details see supplementary material (S3). The probabilistic DBS target for essential tremor in MNI space was overlapped with these atlases and corresponding atlas structures were identified.

To compute whole-brain connectivity of the MNI-space DBS target for essential tremor, we took advantage of publically available functional and anatomical connectomes in MNI space. Resting-state functional connectivity data came from a database of 1000 subjects (Thomas Yeo et al., 2011). BOLD time series from the probabilistic DBS target for essential tremor in MNI space was isolated from the rs-fMRI data of each subject and correlated to each voxel's time series (Fox et al., 2014). Average R-values across subjects were calculated for each voxel and fMRI mappings were visualized using Surf Ice software (https://www.nitrc.org/projects/surfice/).

Structural connectivity utilized a database of diffusion spectrum and T2-weighted imaging from 32 subjects, part of the Human Connectome Project (HCP) at Massachusetts General Hospital ("MGH HCP Adult Diffusion"; Setsompop et al., 2013; https://ida.loni.usc.edu/login.jsp). Data was processed using a generalized q-sampling imaging algorithm (Yeh et al., 2010) as implemented in DSI studio (http://dsi-studio.labsolver.org). A white matter mask was estimated by segmenting the T2-weighted anatomical images and co-registering the images to the b0 image of the diffusion data using SPM12. In each subject, two-hundred thousand fibers were sampled within this mask. Fibers were transformed into MNI space using Lead-DBS following the approach described in (Horn, 2015; Horn et al., 2013). This was done based on the nonlinear deformation field into MNI space calculated based on T2-weighted images using a diffeomorphic registration

algorithm (Ashburner, 2007). Tractography results were displayed using TrackVis software (http://www.trackvis.org/).

Results

To avoid marking the AC and PC locations by hand in all 450 subjects, we first validated an automated method for automatically marking these locations based on non-linear warping of an atlas (Pallavaram et al., 2015). RMS distance errors between manually-marked and automatically-marked coordinates were 0.29 mm (X-Axis), 1.59 mm (Y-Axis) and 1.16 mm (Z-Axis) for the Young cohort (fig. S1). For DBS patients, results were similar (0.53 mm on X-, 1.27 mm on Y- and 1.33 mm on Z-axis). These errors are on par with the voxel-wise resolution of the MRI data itself (0.7 mm isotropic for the *Young* cohort, 0.5 × 0.5 × 2 mm for the *DBS Patient* cohorts). Pearson's correlation coefficients between manually-marked and automatically-marked X-, Y- and Z- coordinates were above 0.99 in both cohorts.

The AC/PC coordinates of active DBS electrode contacts from 51 PD patients and 9 TRD patients were transformed into MNI space using a variety of different methods (Figure 2). Using the MRI from the actual patient (i.e. the gold standard), MNI coordinates for active contact in the PD patients was x = 12.0, y = -12.4, z = -5.7 mm and for the TRD patients was x = ±7.3, y = 25.3, z = -13.1 mm. When attempting to approximate this transform without using the patient's own MRI, the Talairach to MNI transforms (Brett et al., 2002; Lancaster et al., 2007) and marking of coordinates directly on the MNI template (*MNI survey*) resulted in a single point, while the nonlinear transforms using groups of subjects (*Young, PD Age-matched, PD Disease matched, Other DBS patients*) resulted in a probabilistic distribution in MNI space. The error compared to the gold standard was significantly different across different methods for both the PD and TRD cohorts ($p<0.001$).

In PD patients (where the DBS target resides closer to the AC/PC line), the probabilistic methods significantly outperformed the *Tal2MNI* and *Tal2ICBM* methods ($P<0.05$) but not the *MNI survey* method. Surprisingly, the *MNI survey* method actually performed better

than the probabilistic mapping using the young cohort, likely because the larger MNI brain better matches lateral displacement of the STN with age (see fig. S2). Amongst the probabilistic methods, there was a trend towards less error using cohorts increasingly similar to the PD DBS patients themselves, however differences were small (< 0.5 mm) and not statistically significant ($P > 0.07$ for all head-to-head comparisons). In TRD patients (where the DBS target is further from the AC/PC line) the probabilistic methods significantly outperformed the *MNI survey* and *Tal2MNI* methods ($P>0.05$) but not the *Tal2ICBM* method. There was no difference between the three probabilistic methods (*Young* vs. *Age Matched* vs. *other TRD DBS patients*).

Although the *MNI survey* method performed well in the PD DBS group and the *Tal2ICBM* method performed well in the TRD DBS group, only the probabilistic method performed well in both groups. Furthermore, the variance of probabilistic mappings was significantly different in x-, y- and z-directions ($\chi2 = 52.1$, $p<0.001$ for PD, $\chi2 = 10.4$, $p<0.006$ for TRD, based on *Age matched* cohort). In PD variance along the x-axis was significantly higher than along y- ($F = 0.26$, $p<0.001$) and z- axes ($F=0.17$, $p<0.001$). In TRD, variance along the z-axis was significantly lower than for x- ($F=0.21$, $p<0.003$) and y-axes ($F=0.36$, $p<0.05$). Using different cohorts for probabilistic mappings yielded comparable results. This illustrates that depending on the DBS target, variance of the probabilistic mapping approach yields differently shaped non-spherical probability maps in MNI space.

Based on the above results, we next used probabilistic mapping with age-matched cohorts to convert previously reported AC/PC DBS electrode coordinates into probabilistic MNI coordinates across a variety of different diseases (Figure 3, Table 1). X-, y- and z-coordinates were normally distributed across warps from the age-matched cohort at the 5% significance level. Single warps are superimposed as Asterisks over a fitted Gaussian distribution is visualized, for each target.

Once DBS targets are mapped in a probabilistic fashion into MNI space, they can be combined with a number of MNI-based neuroimaging resources. As an example, the DBS target for Essential Tremor (conventionally the ventral intermediate nucleus, VIM, of the thalamus) is illustrated in figure 4. The DBS target was overlaid on five thalamic atlases available in MNI space (figure 4A). The Chakravarty atlas showed the target in the anterior portion of the ventral posterior lateral nucleus (VPLa), whereas the Morel atlas showed it in the ventral posterior medial nucleus (VPM). Both nuclei are directly adjacent to the ventral part of the ventral lateral posterior nucleus (VLpv) which (in Hirai & Jones nomenclature) corresponds to the VIM (in Walker nomenclature) or Vimi (in Hassler nomenclature; Macchi and Jones, 1997). Thalamic parcellations based on anatomical connectivity (Behrens et al., 2003), showed the DBS target in premotor and primary motor zones of the thalamus, while parcellations based on functional connectivity showed it between motor and sensory (Zhang et al., 2008) or in thal-5 zone (Joliot et al., 2015). Finally, the VIM DBS target could be related to histological MNI-based resources such as the BigBrain dataset (Amunts et al., 2013).

Beyond atlases, connectome datasets are also widely available in MNI space and can be used to compute the anatomical and functional connectivity profiles of DBS targets. Our probabilistic DBS target for essential tremor was functionally connected to the motor network and cerebellum (fig. 4B, left) and structurally adjacent to the cerebellothalamocortical pathway (fig. 4B, right).

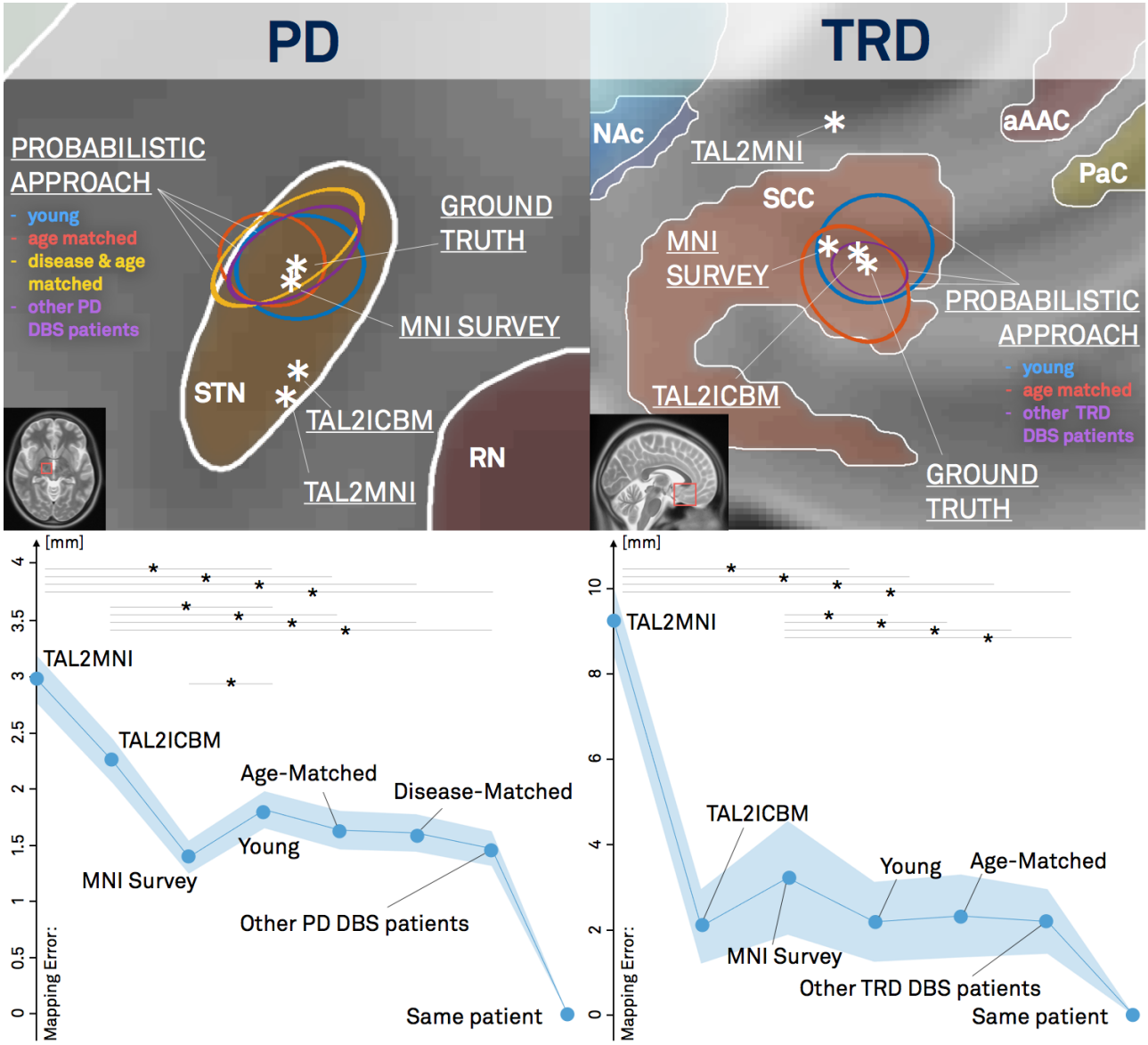

Figure 2 Mapping of active contacts of two DBS cohorts into MNI space using different approaches. Left: cohort of 39 PD patients (target STN). Right: cohort of 9 patients with treatment-refractory major depression (target SCC). For PD, Young, age-matched, disease-matched and disease-severity matched cohorts were available. In case of the depression cohort, the Young, age-matched and original cohort were compared. The upper panels show mappings from group average coordinates of active contacts for both DBS cohorts. The lower panels show mapping errors (compared to the gold standard of manually localized DBS electrode contacts) when active cohorts of all patients were mapped independently. In PD, the probabilistic methods significantly outperformed all

methods except the *MNI survey* method, whereas in TRD, they outperformed all methods except the *Tal2ICBM* method (stars indicate $p<0.05$).

Table 1: AC/PC and transformed MNI coordinates for common DBS targets. AC/PC coordinates are specified as lateral to, anterior to, and below the reference point (MCP or AC). All coordinates are listed as X, Y, then Z. Mean ages are reported as mean age ± standard deviation (age range). Mappings were performed on an age matched sample of the IXI dataset.

Disease	DBS Target	Reference	Number of patients	Mean age of cohort (yrs)	AC/PC coordinates	Relative to	MNI coordinates	MNI standard deviations
Parkinson's disease	STN	(Caire et al. 2013)	171	59	± 12.02 - 1.53 1.91	MCP	± 12.58 - 13.41 - 5.87	± 0.60 ± 0.71 ± 0.71
Dystonia	GPi	(Starr et al. 2006)	23	32 ± 15	± 20.0 5.8 0.5	MCP	± 22.37 - 5.57 - 4.97	± 1.15 ± 0.91 ± 0.84
Essential tremor	VIM (Thalamus)	(Papavassiliou et al. 2004)	37	66.2 ± 13.6	± 12.8 - 5.7 - 0.8	MCP	± 13.05 - 18.38 - 2.01	± 0.96 ± 0.80 ± 0.64
Treatment-resistant depression *	Subcallosal cingulate	(Hamani et al. 2009)	20	50.11 **	± 5.6 34.2 3.0	MCP	± 7.35 23.75 - 11.60	± 0.95 ± 2.14 ± 1.79
Obsessive-compulsive disorder	NAc	(Franzini et al. 2010)	2	37 ± 5.6 (33 – 41)	± 3 16 2	MCP	± 3.78 5.08 - 7.79	± 0.44 ± 0.91 ± 0.30

	ALIC	(Nuttin et al. 2003) (Anderson & Ahmed 2003)	6	35 ***	± 14.00 6.0 - 6.0	AC	± 15.29 8.08 1.57	± 1.04 ± 0.92 ± 0.86
Tourette's syndrome	CM/Pv/VOl (Thalamus)	(Ackermans et al. 2011)	8	40.33 (35 – 48)	± 5.0 4.0 0.0	MCP	± 5.54 - 15.81 - 3.25	± 1.15 ± 1.05 ± 0.50
Alzheimer's disease	Fornix	(Ponce et al. 2015)	42	68.2 ± 7.8 (48.0 – 79.7)	± 4.4 9.8 7.2	MCP	± 4.94 - 1.52 - 13.98	± 0.47 ± 1.06 ± 0.75
Addiction	NAc	(Müller et al. 2009)	3	37.7 ± 2.1 (36 – 40)	± 6.5 2.7 4.5	AC	± 7.66 3.61 - 10.35	± 0.66 ± 0.39 ± 0.49

* for TRD, DBS coordinates have been reported directly within MNI space in {RivaPosse 2014cea} – see discussion

** The age of the cohort in Hamani et al. 2009 could not be retrieved. The mean age of the study by Merkl et al. 2013 was used instead

*** The age of the cohort in Nuttin et al. 2003 could not be retrieved. The mean age from Anderson & Ahmed 2003 was used instead.

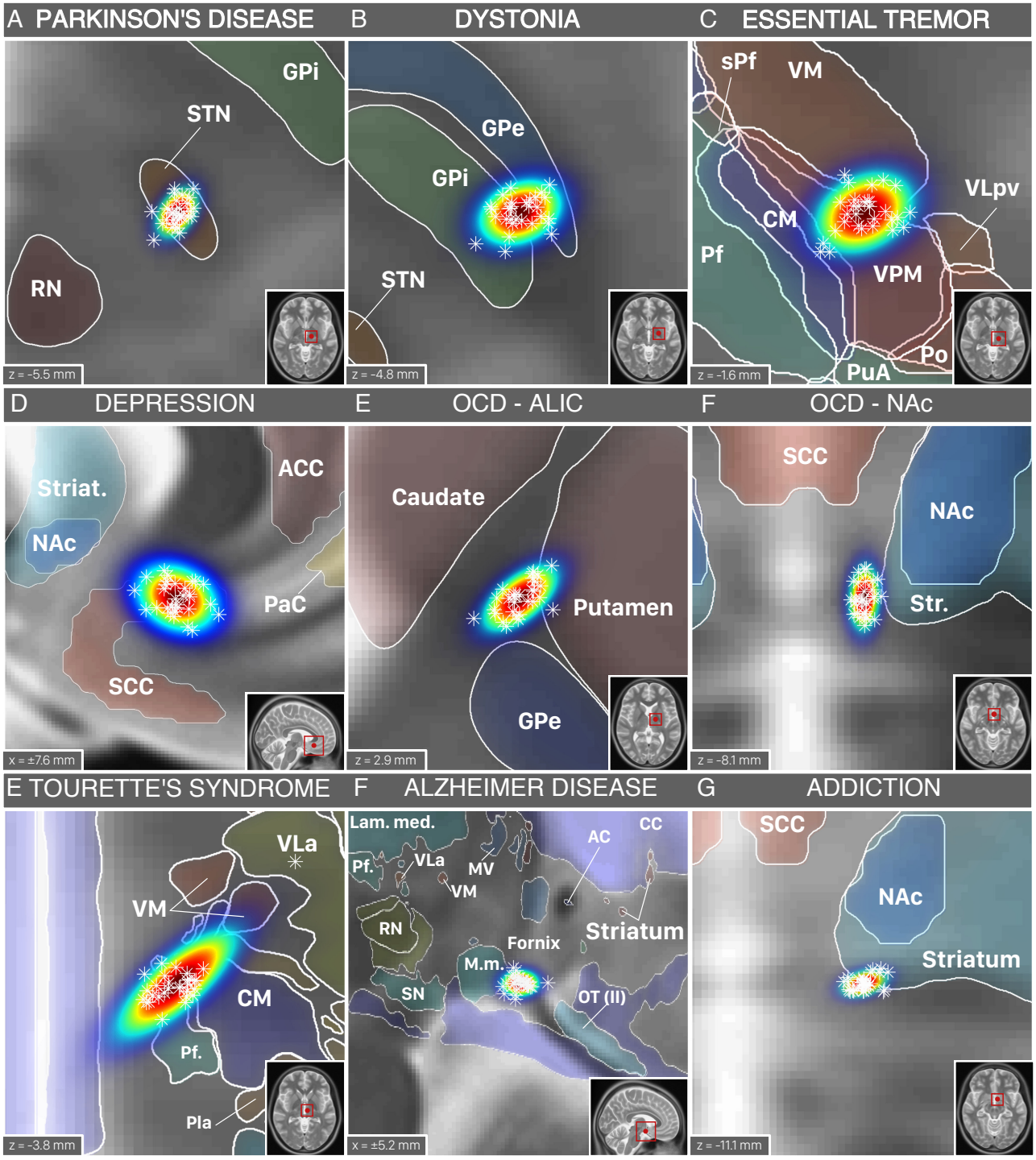

Figure 3: Spatial location of probabilistic DBS targets (table 1) in synopsis with structural brain atlases available in MNI space. Parkinson‘s disease (STN; A) and Dystonia (GPi; B) targets shown with structures defined by DISTAL atlas (Ewert and Horn, 2016). Essential tremor target (VIM; C) shown with Morel atlas structures. Depression (SCC; D), OCD (NAc; F) and Addiction (NAc; G) targets shown with structures from the Harvard-Oxford atlas (Desikan et al., 2006) and the striatum ROI from the ATAG atlas (Keuken et al.,

2014). OCD target in the ALIC shown with structures defined by the ATAG atlas (Keuken et al., 2014). DBS targets for Tourette‘s syndrome (CM/Pv/VOI; E) and Alzheimer‘s disease (Fornix; F) shown with structures from the Chakravarty atlas (Chakravarty et al., 2006). For abbreviations see (Chakravarty et al., 2006; Krauth et al., 2010); thalamic nuclei were labeled using Jones nomenclature whenever possible (Macchi and Jones, 1997) and Hassler nomenclature for nuclei not defined in Jones nomenclature (Hassler et al., 1965; Schaltenbrand et al., 1977).

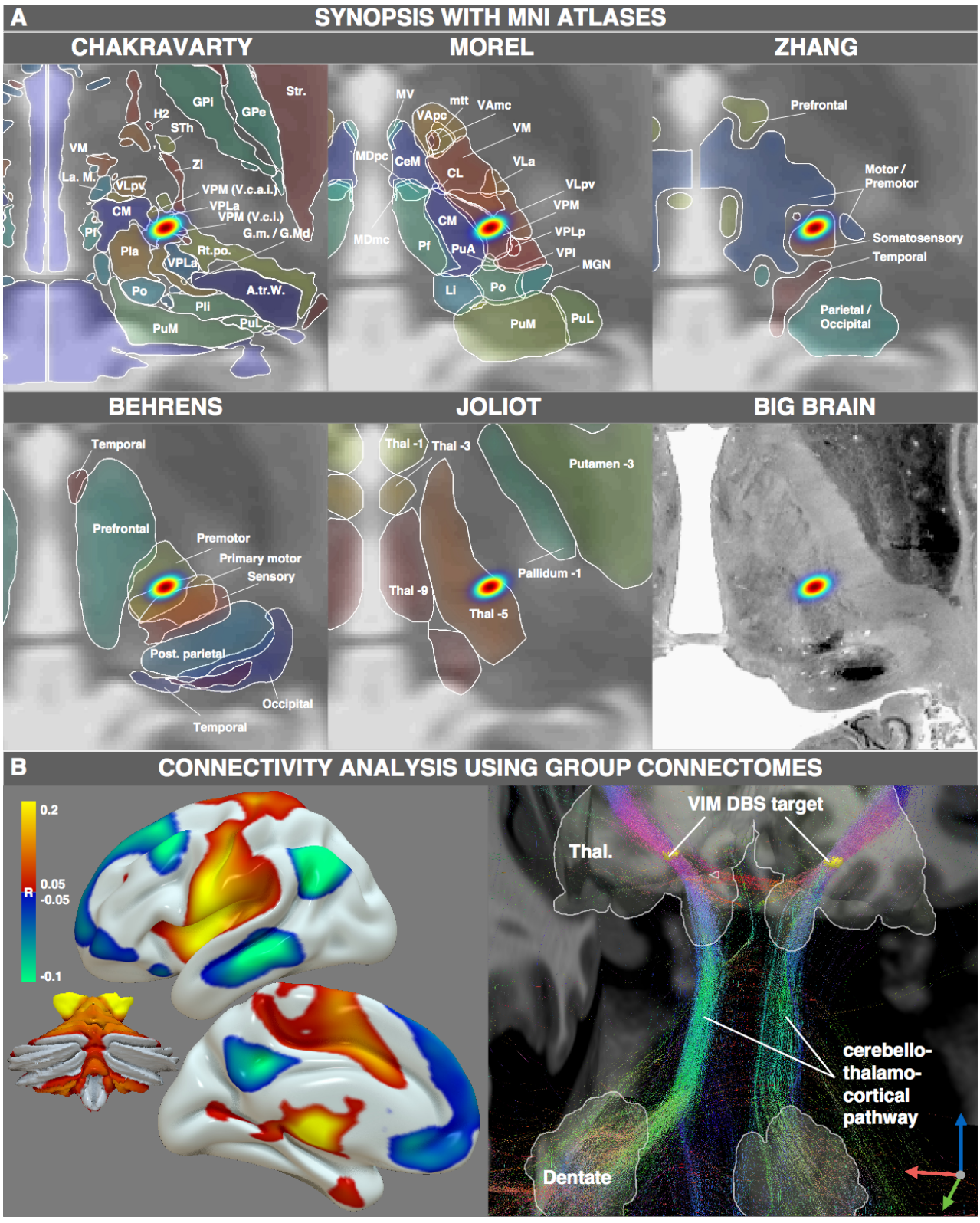

Figure 4: MNI resources that may be used once the DBS target is available in standard space. A) synopsis of the VIM DBS target with five structural atlases available in MNI space. B) Functional (left) and structural (right) connectivity analysis seeding from the VIM DBS target.

Discussion

There are three main findings from this study. First, we presented and validated a conversion tool to map from AC/PC coordinates to MNI space in a probabilistic fashion by taking individual anatomical variation into account. Second, we used this tool to identify MNI coordinates for classical DBS targets defined in the literature. Finally, we demonstrate the utility of integrating DBS lead locations with MNI-based resources, using the DBS target for essential tremor as an example. Implications of each finding and its limitations will be discussed in turn.

Although there are existing well-validated tools for converting Talairach coordinates to MNI space (Laird et al., 2010; Lancaster et al., 2007), the current method provides two advantages. First, it was designed and tested for accuracy using DBS electrode positions, overcoming unique challenges like converting MCP to AC-based coordinates. Second, our method is probabilistic, incorporating anatomic variability into the transform. Rather than identify a single point in MNI space, our method returns a weighted distribution which significantly varies in the x, y, and z directions and better reflects the most likely location of an electrode contact in MNI space.

The one instance in which our probabilistic approach failed to perform well was using a young cohort to convert STN DBS coordinates. In this case, directly measuring the coordinates on the MNI template was more accurate, likely due to a more lateral STN in elderly patients (Keuken et al., 2013) matching the STN position in the larger MNI brain (fig. S2). This problem resolved when using an age-matched rather than the young cohort for probabilistic mapping. No approach significantly out-performed probabilistic mapping with an age-matched cohort, justifying it's use across diseases (Table 1). However, there was a trend towards more accuracy with better-matched MRIs, and these coordinates may be refined in future work using cohorts matched to each specific disease population.

Similarly, our method was validated for STN DBS for Parkinson's disease and SCC DBS for treatment resistant depression. The use of two different DBS populations is a strength of this study, but other diseases with greater changes in anatomy (e.g. Alzheimer's) may benefit more from transforms better matched to the DBS patient population. A potential limitation is the low number of patients within the SCC cohort (N=9).

There have been prior attempts to identify MNI coordinates of some of the DBS electrode locations investigated here (Höflich et al., 2010). In most cases this was done using manual visual transformation to an MNI atlas (Höflich et al., 2010). Direct transformation of each DBS patient's MRI into MNI space is the gold-standard for identifying MNI coordinates of DBS electrode locations, but this is rarely done in the neurosurgical literature. For example, all of the DBS clinical trials included in table 1 reported coordinates in AC/PC space, but not in MNI space. Comparing MNI coordinates from these prior studies (utilizing our probabilistic transform) to gold standard MNI coordinates identified using the current PD and TRD cohorts, the two match well.

Probabilistic mapping may be seen as a further advantage to bridge the gap between studies of the functional neurosurgery literature and neuroimaging (Fox et al., 2014), because resulting maps may be used to analyze the spatial positions based on anatomical atlases and their structural and functional connectivity in a probabilistic manner (by applying them as weighted seeds to standardized connectomes in MNI space). This was demonstrated using the ET DBS target. Using this method, the VIM target defined by (Papavassiliou et al., 2004) and colleagues resided within the ventral posterior medial nucleus based on both Morel and Chakravarty atlases (nuclei defined in Jones nomenclature (Macchi and Jones, 1997)). The VPM nucleus resides directly adjacent to the VLpv nucleus which in Jones nomenclature corresponds to the VIM in Hassler/Walker nomenclatures.

Functional connectivity of the VIM DBS target was analyzed previously in a study by Fox and colleagues (Fox et al., 2014). However, in that study the DBS target was defined anatomically (VLpv ≈ VIM/v.im.i nucleus defined by the Chakravarty atlas) rather than based on the location of effective DBS electrode contacts. As such, the results of the present study differ slightly from this prior work: there are stronger correlations with primary motor cortex and weaker correlations with the superior frontal gyrus. These new results align better with prior work showing that functional connectivity from primary motor cortex (and cerebellum) aligns well with thalamic DBS targets (J. S. Anderson et al., 2011). The current results illustrate that using actual DBS electrode locations instead of anatomically defined ROIs as seed regions in connectivity experiments may make a difference. This is especially important given the increasing interest of the DBS research community in connectivity analyses (Accolla et al., 2016; Henderson, 2012; Vanegas Arroyave et al., 2016).

Regarding structural connectivity, the VLp (≈ VIM) nucleus of the thalamus was initially defined as the large-celled cerebellar recipient zone by Jones (Krack et al., 2002; Macchi and Jones, 1997; its ventral part best corresponds to the VIM based on other nomenclatures). The fiber bundle connecting the cerebellar nuclei to the thalamus has been referred to as the dentatothalamic tract, dentatorubrothalamic tract, or cerebellothalamocortical pathway and matches the present results based on connectivity with the thalamic DBS target. Interestingly, most fibers in this pathway are thought to decussate between the thalamus and cerebellum, with only a minority of fibers staying uncrossed (Chan-Palay, 1977; Meola et al., 2015; R. Wiesendanger and M. Wiesendanger, 1985). Whether the predominantly uncrossed tracts identified here are due to the exact position of the electrode with the thalamus (Meola et al., 2015; 2016) or a limitation of DTI requires further work. Either way, this demonstrates the type of analyses that can be performed once the MNI coordinates of DBS electrode positions are known.

It should be noted that the ideal way to convert AC/PC coordinates to MNI space is by using MRI data from the patients themselves. Unfortunately, obtaining MRIs from prior studies – especially if multiple studies or large cohorts are concerned – can be difficult if not impossible. In these cases, probabilistic transformation using a surrogate cohort as described here may be useful. Our data shows, that closely matching the original cohort by age, disease and even disease severity does improve results (although only age-matching improved results significantly). Thus, we argue that matching the original cohort as closely as possible is important.

One other limitation is that often, the explicit methodology of defining the AC and PC fiducials is not reported in original studies (see. fig. 1; Weiss et al., 2003). Here, we incorporated the most common approach, i.e. defining the posterior border of the AC and the anterior of the PC. However, our algorithm should be modified if surgeons in an original study of interest used a different approach for marking the AC and PC.

Conclusions

We introduced a method for converting stereotactic AC/PC coordinates to MNI space in a probabilistic fashion that incorporates anatomic variability. Our method was validated using two cohorts of DBS patients, appears superior to alternative methods, and works well using transforms derived from healthy subject MRIs. We used this method to convert stereotactic coordinates of common DBS targets into MNI space, providing a resource for future studies. Finally, we use the DBS target for essential tremor as an example to illustrate the value of integrating DBS lead locations with MNI-based resources. The methodology and code will be made available within the open source toolbox Lead-DBS (www.lead-dbs.org).

Acknowledgements

We would like to thank Thomas Yeo, Dongyang Zhang and Abraham Snyder for helpful advice during the preparation of this manuscript.

AH received funding from Stiftung Charité; Berlin Institute of Health and Prof. Klaus Thiemann Foundation. He received travel stipends from Movement Disorders Society and Ipsen Pharma. AAK was supported by the German Research Agency (DFG - Deutsche Forschungsgemeinschaft). Grant Number: KFO 247 and received honoraria from St Jude Medical and Medtronic; travel grants from Ipsen Pharma and Boston Scientific; consultancies from Boston Scientific. AM received a Rahel-Hirsch grant from the Charité and Landesamt für gesundheit und Soziales and was supported by the KFO 247. MDF was supported by grants from the National Institute of Health \ National Institute of Neurologial Disorders and Stroke (K23NS083741), Dystonia Medical Research Foundation, and National Parkinson's Foundation. M.D.F. is listed as inventor on submitted or issued patents on guiding neurological interventions with fMRI.

Data collection and sharing for this project was provided by the Human Connectome Project (HCP; Principal Investigators: Bruce Rosen, M.D., Ph.D., Arthur W. Toga, Ph.D., Van J. Weeden, MD). HCP funding was provided by the National Institute of Dental and Craniofacial Research (NIDCR), the National Institute of Mental Health (NIMH), and the National Institute of Neurological Disorders and Stroke (NINDS). HCP data are disseminated by the Laboratory of Neuro Imaging at the University of Southern California. The HCP project (Principal Investigators: Bruce Rosen, M.D., Ph.D., Martinos Center at Massachusetts General Hospital; Arthur W. Toga, Ph.D., University of Southern California, Van J. Weeden, MD, Martinos Center at Massachusetts General Hospital) is supported by the National Institute of Dental and Craniofacial Research (NIDCR), the National Institute of Mental Health (NIMH) and the National Institute of Neurological Disorders and Stroke

(NINDS). HCP is the result of efforts of co-investigators from the University of Southern California, Martinos Center for Biomedical Imaging at Massachusetts General Hospital (MGH), Washington University, and the University of Minnesota.

Data used in the preparation of this article were obtained from the Parkinson's Progression Markers Initiative (PPMI) database (www.ppmi-info.org/data). For up-to-date information on the study, visit www.ppmi-info.org. PPMI - a public-private partnership - is funded by the Michael J. Fox Foundation for Parkinson's Research and funding partners, see www.ppmi-info.org/fundingpartners.

Bibliography

Accolla, E.A., Herrojo Ruiz, M., Horn, A., Schneider, G.-H., Schmitz-Hubsch, T., Draganski, B., Kühn, A.A., 2016. Brain networks modulated by subthalamic nucleus deep brain stimulation. Brain aww182. doi:10.1093/brain/aww182

Accolla, E. A., Dukart, J., Helms, G., Weiskopf, N., Kherif, F., Lutti, A., et al. (2014). Brain tissue properties differentiate between motor and limbic basal ganglia circuits. Human Brain Mapping. http://doi.org/10.1002/hbm.22533

Ackermans, L., Duits, A., van der Linden, C., Tijssen, M., Schruers, K., Temel, Y., Kleijer, M., Nederveen, P., Bruggeman, R., Tromp, S., van Kranen-Mastenbroek, V., Kingma, H., Cath, D., Visser-Vandewalle, V., 2011. Double-blind clinical trial of thalamic stimulation in patients with Tourette syndrome. Brain 134, 832–844. doi: 10.1093/brain/awq380

Allen, J.S., Damasio, H., Grabowski, T.J., 2002. Normal neuroanatomical variation in the human brain: An MRI-volumetric study. American Journal of Physical Anthropology 118, 341–358. doi:10.1002/ajpa.10092

Amunts, K., Lepage, C., Borgeat, L., Mohlberg, H., Dickscheid, T., Rousseau, M.-É., Bludau, S., Bazin, P.-L., Lewis, L.B., Oros-Peusquens, A.-M., Shah, N.J., Lippert, T., Zilles, K., Evans, A.C., 2013. BigBrain: an ultrahigh-resolution 3D human brain model. Science 340, 1472–1475. doi:10.1126/science.1235381

Anderson, D., Ahmed, A., 2003. Treatment of patients with intractable obsessive—compulsive disorder with anterior capsular stimulation. J Neurosurg 98, 1104–1108. doi:10.3171/jns.2003.98.5.1104

Anderson, J.S., Dhatt, H.S., Ferguson, M.A., Lopez-Larson, M., Schrock, L.E., House, P.A., Yurgelun-Todd, D., 2011. Functional connectivity targeting for deep brain stimulation in essential tremor. AJNR Am J Neuroradiol 32, 1963–1968. doi: 10.3174/ajnr.A2638

Ashburner, J., 2012. SPM: a history.

Ashburner, J., 2007. A fast diffeomorphic image registration algorithm. 38, 95–113. doi: 10.1016/j.neuroimage.2007.07.007

Atkinson, J.D., Collins, D.L., Bertrand, G., Peters, T.M., Pike, G.B., Sadikot, A.F., 2002. Optimal location of thalamotomy lesions for tremor associated with Parkinson disease: a probabilistic analysis based on postoperative magnetic resonance imaging and an integrated digital atlas. J Neurosurg 96, 854–866. doi:10.3171/jns. 2002.96.5.0854

Avants, B.B., Epstein, C.L., Grossman, M., Gee, J.C., 2008. Symmetric diffeomorphic image registration with cross-correlation: evaluating automated labeling of elderly and neurodegenerative brain. Med Image Anal 12, 26–41. doi:10.1016/j.media. 2007.06.004

Barow, E., Neumann, W.-J., Brücke, C., Huebl, J., Horn, A., Brown, P., Krauss, J.K., Schneider, G.-H., Kühn, A.A., 2014. Deep brain stimulation suppresses pallidal low frequency activity in patients with phasic dystonic movements. Brain 137, 3012–3024. doi:10.1093/brain/awu258

Behrens, T.E.J., Johansen-Berg, H., Woolrich, M.W., Smith, S.M., Wheeler-Kingshott, C.A.M., Boulby, P.A., Barker, G.J., Sillery, E.L., Sheehan, K., Ciccarelli, O., Thompson, A.J., Brady, J.M., Matthews, P.M., 2003. Non-invasive mapping of

connections between human thalamus and cortex using diffusion imaging. 6, 750–757. doi:10.1038/nn1075

Benabid, A.L., Pollak, P., Gao, D., Hoffmann, D., Limousin, P., Gay, E., Payen, I., Benazzouz, A., 1996. Chronic electrical stimulation of the ventralis intermedius nucleus of the thalamus as a treatment of movement disorders. J Neurosurg 84, 203–214. doi:10.3171/jns.1996.84.2.0203

Benabid, A.L., Pollak, P., Gervason, C., Hoffmann, D., Gao, D.M., Hommel, M., Perret, J.E., de Rougemont, J., 1991. Long-term suppression of tremor by chronic stimulation of the ventral intermediate thalamic nucleus. Lancet 337, 403–406.

Boes, A. D., Prasad, S., Liu, H., Liu, Q., Pascual-Leone, A., Caviness, V. S., Jr, & Fox, M. D. (2015). Network localization of neurological symptoms from focal brain lesions. Brain : a Journal of Neurology, 138(10), 3061–3075. http://doi.org/10.1093/brain/awv228

Brett, M., Johnsrude, I.S., Owen, A.M., 2002. The problem of functional localization in the human brain. Nat Rev Neurosci 3, 243–249. doi:10.1038/nrn756

Caire, F., Ranoux, D., Guehl, D., Burbaud, P., Cuny, E., 2013. A systematic review of studies on anatomical position of electrode contacts used for chronic subthalamic stimulation in Parkinson's disease. Acta Neurochir (Wien) 155, 1647–54–discussion 1654. doi:10.1007/s00701-013-1782-1

Chakravarty, M.M., Bertrand, G., Hodge, C.P., Sadikot, A.F., Collins, D.L., 2006. The creation of a brain atlas for image guided neurosurgery using serial histological data. NeuroImage 30, 359–376. doi:10.1016/j.neuroimage.2005.09.041

Chan-Palay, V., 1977. Cerebellar Dentate Nucleus. Springer.

Choi, E. Y., Yeo, B. T. T., & Buckner, R. L. (2012). The organization of the human striatum estimated by intrinsic functional connectivity. Journal of Neurophysiology, 108(8), 2242–2263. http://doi.org/10.1152/jn.00270.2012

Clarke, R.H., Horsley, V., 1906. On a method of investigating the deep ganglia and tracts of the central nervous system (cerebellum). Br Med J 463, 1799–1800. doi:10.1097/BLO.0b013e31814d4d99

Collins, D.L., 1994. 3D Model-based Segmentation of Individual Brain Structures from Magnetic Resonance Imaging Data.

Darby, R., Laganiere, S., Pascual-Leone, A., Prasad, S., & Fox, M. D. (2016). Finding the imposter: brain connectivity of lesions causing delusional misidentifications. Brain : a Journal of Neurology, 1–11. http://doi.org/10.1093/brain/aww288

Desikan, R.S., Ségonne, F., Fischl, B., Quinn, B.T., Dickerson, B.C., Blacker, D., Buckner, R.L., Dale, A.M., Maguire, R.P., Hyman, B.T., Albert, M.S., Killiany, R.J., 2006. An automated labeling system for subdividing the human cerebral cortex on MRI scans into gyral based regions of interest. NeuroImage 31, 968–980. doi:10.1016/j.neuroimage.2006.01.021

Diedrichsen, J., Maderwald, S., Küper, M., Thürling, M., Rabe, K., Gizewski, E. R., et al. (2011). Imaging the deep cerebellar nuclei: a probabilistic atlas and normalization procedure. NeuroImage, 54(3), 1786–1794. http://doi.org/10.1016/j.neuroimage.2010.10.035

Van Essen, D. C., Ugurbil, K., Auerbach, E., Barch, D., Behrens, T. E. J., Bucholz, R., et al. (2012). The Human Connectome Project: a data acquisition perspective. NeuroImage, 62(4), 2222–2231. http://doi.org/10.1016/j.neuroimage.2012.02.018

Ewert, S., Plettig, P., Chakravarty M., Kühn AA., Horn, A., 2016. Toward defining deep brain stimulation targets in MNI space: A subcortical atlas based on multimodal MRI, histology and structural connectivity. doi:10.1101/062851

Fiandaca, M.S., Salegio, E.A., Yin, D., Richardson, R.M., Valles, F.E., Larson, P.S., Starr, P.A., Lonser, R.R., Bankiewicz, K.S., 2011. Human/Nonhuman Primate AC-PC Ratio - Considerations for Translational Brain Measurements. J. Neurosci. Methods 196, 124–130. doi:10.1016/j.jneumeth.2010.12.023

Fischer, D. B., Boes, A. D., Demertzi, A., Evrard, H. C., Laureys, S., Edlow, B. L., et al. (2016). A human brain network derived from coma-causing brainstem lesions. Neurology, 10.1212/WNL.0000000000003404–9. http://doi.org/10.1212/WNL.0000000000003404

Fonov, V. S., Evans, A. C., McKinstry, R. C., Almli, C. R., & Collins, D. L. (2009). Unbiased nonlinear average age-appropriate brain templates from birth to adulthood. NeuroImage, 47, S102.

Fox, M.D., Buckner, R.L., Liu, H., Chakravarty, M.M., Lozano, A.M., Pascual-Leone, A., 2014. Resting-state networks link invasive and noninvasive brain stimulation across diverse psychiatric and neurological diseases. Proceedings of the National Academy of Sciences 111, E4367–75. doi:10.1073/pnas.1405003111

Franzini, A., Messina, G., Gambini, O., Muffatti, R., Scarone, S., Cordella, R., Broggi, G., 2010. Deep-brain stimulation of the nucleus accumbens in obsessive compulsive disorder: clinical, surgical and electrophysiological considerations in two consecutive patients. Neurol Sci 31, 353–359. doi:10.1007/s10072-009-0214-8

Goldman, M.S., Ahlskog, J.E., Kelly, P.J., 1992. The symptomatic and functional outcome of stereotactic thalamotomy for medically intractable essential tremor. J Neurosurg 76, 924–928. doi:10.3171/jns.1992.76.6.0924

Grabner, G., Poser, B.A., Fujimoto, K., Polimeni, J.R., Wald, L.L., Trattnig, S., Toni, I., Barth, M., 2014. A study-specific fMRI normalization approach that operates directly on high resolution functional EPI data at 7 Tesla. - PubMed - NCBI. NeuroImage 100, 710–714.

Groppa, S., Herzog, J., Falk, D., Riedel, C., Deuschl, G., Volkmann, J., 2014. Physiological and anatomical decomposition of subthalamic neurostimulation effects in essential tremor. 137, 109–121. doi:10.1093/brain/awt304

Guiot, G., Arfel, G., Derome, P., 1968. Guiot: La chirurgie stéréotaxique des tremblements... - Google Scholar. Gaz Med.

Hamani, C., Mayberg, H., Snyder, B., Giacobbe, P., Kennedy, S., Lozano, A.M., 2009. Deep brain stimulation of the subcallosal cingulate gyrus for depression: anatomical location of active contacts in clinical responders and a suggested guideline for targeting. J Neurosurg 111, 1209–1215. doi:10.3171/2008.10.JNS08763

Hamani, C., Richter, E., Schwalb, J.M., Lozano, A.M., 2005. Bilateral subthalamic nucleus stimulation for Parkinson's disease: a systematic review of the clinical literature. Neurosurgery 56, 1313–21– discussion 1321–4.

Hamel, W., Herzog, J., Kopper, F., Pinsker, M., Weinert, D., Müller, D., Krack, P., Deuschl, G., Mehdorn, H.M., 2007. Deep brain stimulation in the subthalamic area is more effective than nucleus ventralis intermedius stimulation for bilateral intention tremor. Acta Neurochir (Wien) 149, 749–58– discussion 758. doi:10.1007/s00701-007-1230-1

Hassler, R., Mundinger, F., Riechert, T., 1965. Correlations between clinical and autoptic findings in stereotaxic operations of parkinsonism. Confin Neurol 26, 282–290.

Henderson, J.M., 2012. “Connectomic surgery”: diffusion tensor imaging (DTI) tractography as a targeting modality for surgical modulation of neural networks. Front Integr Neurosci 6, 15. doi:10.3389/fnint.2012.00015

Hohlefeld, F.U., Ehlen, F., Tiedt, H.O., Krugel, L.K., Horn, A., Kühn, A.A., Curio, G., Klostermann, F., Nikulin, V.V., 2015. Correlation between cortical and subcortical neural dynamics on multiple time scales in Parkinson's disease. Neuroscience 298, 145–160. doi:10.1016/j.neuroscience.2015.04.013

Horn, A., 2015. A structural group-connectome in standard stereotactic (MNI) space. NeuroImage 5, 292–296. doi:10.1016/j.dib.2015.08.035

Horn, A., Kühn, A.A., 2015. Lead-DBS: a toolbox for deep brain stimulation electrode localizations and visualizations. NeuroImage 107, 127–135. doi:10.1016/j.neuroimage.2014.12.002

Horn, A., Ostwald, D., Reisert, M., Blankenburg, F., 2013. The structural-functional connectome and the default mode network of the human brain. 102, 142–151. doi:10.1016/j.neuroimage.2013.09.069

Höflich, A., Savli, M., Comasco, E., Moser, U., Novak, K., Kasper, S., Lanzenberger, R., 2010. Neuropsychiatric deep brain stimulation for translational neuroimaging. NeuroImage 79, 1–12. doi:10.1016/j.neuroimage.2013.04.065

Jakab, A., Blanc, R., Berenyi, E.L., Szekely, G., 2012. Generation of Individualized Thalamus Target Maps by Using Statistical Shape Models and Thalamocortical Tractography. AJNR Am J Neuroradiol 33, 2110–2116. doi:10.3174/ajnr.A3140

Joliot, M., Jobard, G., Naveau, M., Delcroix, N., Petit, L., Zago, L., Crivello, F., Mellet, E., Mazoyer, B., Tzourio-Mazoyer, N., 2015. AICHA: An atlas of intrinsic connectivity of homotopic areas. J. Neurosci. Methods 254, 46–59. doi:10.1016/j.jneumeth.2015.07.013

Keuken, M.C., Bazin, P.-L., Schäfer, A., Neumann, J., Turner, R., Forstmann, B.U., 2013. Ultra-high 7T MRI of structural age-related changes of the subthalamic nucleus. 33, 4896–4900. doi:10.1523/JNEUROSCI.3241-12.2013

Keuken, M.C., Bazin, P.L., Crown, L., Hootsmans, J., Laufer, A., Müller-Axt, C., Sier, R., van der Putten, E.J., Schäfer, A., Turner, R., Forstmann, B.U., 2014. Quantifying inter-individual anatomical variability in the subcortex using 7T structural MRI 94, 40–46. doi:10.1016/j.neuroimage.2014.03.032

Klein, A., Andersson, J., Ardekani, B.A., Ashburner, J., Avants, B., Chiang, M.-C., Christensen, G.E., Collins, D.L., Gee, J., Hellier, P., Song, J.H., Jenkinson, M., Lepage, C., Rueckert, D., Thompson, P., Vercauteren, T., Woods, R.P., Mann, J.J., Parsey, R.V., 2009. Evaluation of 14 nonlinear deformation algorithms applied to human brain MRI registration. 46, 786–802. doi:10.1016/j.neuroimage.2008.12.037

Krack, P., Dostrovsky, J., Ilinsky, I., Kultas-Ilinsky, K., Lenz, F., Lozano, A., Vitek, J., 2002. Surgery of the motor thalamus: Problems with the present nomenclatures. Mov. Disord. 17, S2–S8. doi:10.1002/mds.10136

Krauth, A., Blanc, R., Poveda, A., Jeanmonod, D., Morel, A., Székely, G., 2010. A mean three-dimensional atlas of the human thalamus: generation from multiple histological data. 49, 2053–2062. doi:10.1016/j.neuroimage.2009.10.042

Kühn, A.A., Volkmann, J., 2016. Innovations in deep brain stimulation methodology. Movement Disorders. doi:10.1002/mds.26703

Kuklisova-Murgasova, M., Aljabar, P., Srinivasan, L., Counsell, S. J., Doria, V., Serag, A., et al. (2011). A dynamic 4D probabilistic atlas of the developing brain. NeuroImage, 54(4), 2750–2763. http://doi.org/10.1016/j.neuroimage.2010.10.019

Lacadie, C.M., Fulbright, R.K., Rajeevan, N., Constable, R.T., Papademetris, X., 2008. More accurate Talairach coordinates for neuroimaging using non-linear registration. NeuroImage 42, 717–725. doi:10.1016/j.neuroimage.2008.04.240

Laganiere, S., Boes, A. D., & Fox, M. D. (2016). Network localization of hemichorea-hemiballismus. Neurology, 86(23), 2187–2195. http://doi.org/10.1212/WNL.0000000000002741

Laird, A.R., Robinson, J.L., McMillan, K.M., Tordesillas-Gutiérrez, D., Moran, S.T., Gonzales, S.M., Ray, K.L., Franklin, C., Glahn, D.C., Fox, P.T., Lancaster, J.L., 2010. Comparison of the disparity between Talairach and MNI coordinates in functional neuroimaging data: Validation of the Lancaster transform. NeuroImage 51, 677–683. doi:10.1016/j.neuroimage.2010.02.048

Lancaster, J.L., Tordesillas-Gutiérrez, D., Martinez, M., Salinas, F., Evans, A., Zilles, K., Mazziotta, J.C., Fox, P.T., 2007. Bias between MNI and Talairach coordinates analyzed using the ICBM-152 brain template. Hum Brain Mapp 28, 1194–1205. doi: 10.1002/hbm.20345

Lee, T.-O., Hwang, H.-S., De Salles, A., Mattozo, C., Pedroso, A.G., Behnke, E., 2008. Inter-racial, gender and aging influences in the length of anterior commissure-posterior commissure line. J Korean Neurosurg Soc 43, 79–84. doi:10.3340/jkns.2008.43.2.79

Liang, P., Shi, L., Chen, N., Luo, Y., Wang, X., Liu, K., Mok, V.C., Chu, W.C., Wang, D., Li, K., 2015. Construction of brain atlases based on a multi-center MRI dataset of 2020 Chinese adults. Scientific Reports 5, 18216. doi:10.1038/srep18216

Lozano, A.M., Lipsman, N., 2013. Probing and Regulating Dysfunctional Circuits Using Deep Brain Stimulation 77, 406–424. doi:10.1016/j.neuron.2013.01.020

Luigjes, J., van den Brink, W., Feenstra, M., van den Munckhof, P., Schuurman, P.R., Schippers, R., Mazaheri, A., De Vries, T.J., Denys, D., 2011. Deep brain stimulation in addiction: a review of potential brain targets. Mol Psychiatry 17, 572–583. doi: 10.1038/mp.2011.114

Macchi, G., Jones, E.G., 1997. Toward an agreement on terminology of nuclear and subnuclear divisions of the motor thalamus. J Neurosurg 86, 77–92. doi:10.3171/jns.1997.86.1.0077

Mayberg, H.S., Lozano, A.M., Voon, V., McNeely, H.E., Seminowicz, D., Hamani, C., Schwalb, J.M., Kennedy, S.H., 2005. Deep brain stimulation for treatment-resistant depression. 45, 651–660. doi:10.1016/j.neuron.2005.02.014

Meola, A., Comert, A., Yeh, F.-C., Sivakanthan, S., Fernandez-Miranda, J.C., 2015. The nondecussating pathway of the dentatorubrothalamic tract in humans: human connectome-based tractographic study and microdissection validation. J Neurosurg 1–7. doi:10.3171/2015.4.JNS142741

Meola, A., Yeh, F.-C., Fellows-Mayle, W., Weed, J., Fernandez-Miranda, J.C., 2016. Human Connectome-Based Tractographic Atlas of the Brainstem Connections and Surgical Approaches. Neurosurgery 1. doi:10.1227/NEU.0000000000001224

Merkl, A., Neumann, W.-J., Huebl, J., Aust, S., Horn, A., Krauss, J.K., Dziobek, I., Kuhn, J., Schneider, G.-H., Bajbouj, M., Kühn, A.A., 2015. Modulation of Beta-Band Activity in

the Subgenual Anterior Cingulate Cortex during Emotional Empathy in Treatment-Resistant Depression. Cereb. Cortex. doi:10.1093/cercor/bhv100

Merkl, A., Schneider, G.-H., Schönecker, T., Aust, S., Kühl, K.-P., Kupsch, A., Kühn, A.A., Bajbouj, M., 2013. Antidepressant effects after short-term and chronic stimulation of the subgenual cingulate gyrus in treatment-resistant depression. Exp. Neurol. 249C, 160–168. doi:10.1016/j.expneurol.2013.08.017

Mobin, F., De Salles, A.A.F., Behnke, E.J., Frysinger, R., 2000. Correlation between MRI-Based Stereotactic Thalamic Deep Brain Stimulation Electrode Placement, Macroelectrode Stimulation and Clinical Response to Tremor Control. Stereotact Funct Neurosurg 72, 225–232. doi:10.1159/000029730

Morel, A., 2013. Stereotactic Atlas of the Human Thalamus and Basal Ganglia. CRC Press.

Mori, S., Oishi, K., Jiang, H., Jiang, L., Li, X., Akhter, K., Hua, K., Faria, A.V., Mahmood, A., Woods, R., Toga, A.W., Pike, G.B., Neto, P.R., Evans, A., Zhang, J., Huang, H., Miller, M.I., van Zijl, P., Mazziotta, J., 2008. Stereotaxic white matter atlas based on diffusion tensor imaging in an ICBM template. 40, 570–582. doi:10.1016/j.neuroimage.2007.12.035

Murata, J.-I., Kitagawa, M., Uesugi, H., Saito, H., Iwasaki, Y., Kikuchi, S., Tashiro, K., Sawamura, Y., 2003. Electrical stimulation of the posterior subthalamic area for the treatment of intractable proximal tremor. J Neurosurg 99, 708–715. doi:10.3171/jns.2003.99.4.0708

Müller, U.J., Sturm, V., Voges, J., Heinze, H.J., Galazky, I., Heldmann, M., Scheich, H., Bogerts, B., 2009. Successful treatment of chronic resistant alcoholism by deep

brain stimulation of nucleus accumbens: first experience with three cases. - PubMed - NCBI. Pharmacopsychiatry 42, 288–291. doi:10.1055/s-0029-1233489

Nestor, K.A., Jones, J.D., Butson, C.R., Morishita, T., Jacobson, C.E., IV, Peace, D.A., Chen, D., Foote, K.D., Okun, M.S., 2014. Coordinate-Based Lead Location Does Not Predict Parkinson's Disease Deep Brain Stimulation Outcome. PLoS ONE 9, e93524. doi:10.1371/journal.pone.0093524

Neumann, W.-J., Jha, A., Bock, A., Huebl, J., Horn, A., Schneider, G.-H., Sander, T.H., Litvak, V., Kühn, A.A., 2015a. Cortico-pallidal oscillatory connectivity in patients with dystonia. Brain 138, 1894–1906. doi:10.1093/brain/awv109

Neumann, W.-J., Staub, F., Horn, A., Schanda, J., Mueller, J., Schneider, G.-H., Brown, P., Kühn, A.A., 2015b. Deep Brain Recordings Using an Implanted Pulse Generator in Parkinson's Disease. Neuromodulation: Technology at the Neural Interface. doi: 10.1111/ner.12348

Nuttin, B.J., Gabriëls, L.A., Cosyns, P.R., Meyerson, B.A., Andréewitch, S., Sunaert, S.G., Maes, A.F., Dupont, P.J., Gybels, J.M., Gielen, F., Demeulemeester, H.G., 2003. Long-term electrical capsular stimulation in patients with obsessive-compulsive disorder. Neurosurgery 52, 1263–72– discussion 1272–4.

Pallavaram, S., D'Haese, P.-F., Lake, W., Konrad, P.E., Dawant, B.M., Neimat, J.S., 2015. Fully automated targeting using non-rigid image registration matches accuracy and exceeds precision of best manual approaches to Subthalamic Deep Brain Stimulation targeting in Parkinson's disease. Neurosurgery 76, 756–765. doi: 10.1227/NEU.0000000000000714

Pallavaram, S., Yu, H., Spooner, J., D'Haese, P.-F., Bodenheimer, B., Konrad, P.E., Dawant, B.M., 2008. Intersurgeon variability in the selection of anterior and

posterior commissures and its potential effects on target localization. Stereotact Funct Neurosurg 86, 113–119. doi:10.1159/000116215

Papavassiliou, E., Rau, G., Heath, S., Abosch, A., Barbaro, N.M., Larson, P.S., Lamborn, K., Starr, P.A., 2004. Thalamic deep brain stimulation for essential tremor: relation of lead location to outcome. Neurosurgery 54, 1120–29– discussion 1129–30. doi: 10.1227/01.NEU.0000119329.66931.9E

Piedad, J.C.P., Rickards, H.E., Cavanna, A.E., 2012. What patients with gilles de la tourette syndrome should be treated with deep brain stimulation and what is the best target? Neurosurgery 71, 173–192. doi:10.1227/NEU.0b013e3182535a00

Pilitsis, J.G., Metman, L.V., Toleikis, J.R., Hughes, L.E., Sani, S.B., Bakay, R.A.E., 2008. Factors involved in long-term efficacy of deep brain stimulation of the thalamus for essential tremor. J Neurosurg 109, 640–646. doi:10.3171/JNS/2008/109/10/0640

Ponce, F.A., Asaad, W.F., Foote, K.D., Anderson, W.S., Rees Cosgrove, G., Baltuch, G.H., Beasley, K., Reymers, D.E., Oh, E.S., Targum, S.D., Smith, G.S., Lyketsos, C.G., Lozano, A.M., 2015. Bilateral deep brain stimulation of the fornix for Alzheimer's disease: surgical safety in the ADvance trial. J Neurosurg 1–10.

Richter, E.O., Hoque, T., Halliday, W., Lozano, A.M., Saint-Cyr, J.A., 2004. Determining the position and size of the subthalamic nucleus based on magnetic resonance imaging results in patients with advanced Parkinson disease. J Neurosurg 100, 541–546. doi:10.3171/jns.2004.100.3.0541

Riva-Posse, P., Choi, K.S., Holtzheimer, P.E., McIntyre, C.C., Gross, R.E., Chaturvedi, A., Crowell, A.L., Garlow, S.J., Rajendra, J.K., Mayberg, H.S., 2014. Defining critical white matter pathways mediating successful subcallosal cingulate deep brain

stimulation for treatment-resistant depression. Biol. Psychiatry 76, 963–969. doi: 10.1016/j.biopsych.2014.03.029

Schaltenbrand, G., Wahren, W., Hassler, R., 1977. Atlas for Stereotaxy of the Human Brain. Thieme Medical Publishers.

Schmitz-Hubsch, T., Schneider, G.-H., Horn, A., Krause, P., Gruber, D., Nickels, E., Lipp, A., Faust, K., Voges, J., Kühn, A.A., Kupsch, A., 2014. The caudal zona incerta does not prove suitable as a target for deep brain stimulation in Parkinson‘s disease, in:. Presented at the International Parkinson and Movement Disorder Society MDS, San Diego, pp. 1–2.

Schönecker, T., Kupsch, A., Kühn, A.A., Schneider, G.-H., Hoffmann, K.T., 2009. Automated Optimization of Subcortical Cerebral MR Imaging-Atlas Coregistration for Improved Postoperative Electrode Localization in Deep Brain Stimulation. AJNR Am J Neuroradiol 30, 1914–1921. doi:10.3174/ajnr.A1741

Schrock, L.E., Mink, J.W., Woods, D.W., Porta, M., Servello, D., Visser-Vandewalle, V., Silburn, P.A., Foltynie, T., Walker, H.C., Shahed-Jimenez, J., Savica, R., Klassen, B.T., Machado, A.G., Foote, K.D., Zhang, J.-G., Hu, W., Ackermans, L., Temel, Y., Mari, Z., Changizi, B.K., Lozano, A., Auyeung, M., Kaido, T., Agid, Y., Welter, M.L., Khandhar, S.M., Mogilner, A.Y., Pourfar, M.H., Walter, B.L., Juncos, J.L., Gross, R.E., Kuhn, J., Leckman, J.F., Neimat, J.A., Okun, M.S., Tourette Syndrome Association International Deep Brain Stimulation (DBS) Database and Registry Study Group, 2014. Tourette syndrome deep brain stimulation: a review and updated recommendations. - PubMed - NCBI. Mov. Disord. 30, 448–471.

Schroll, H., Horn, A., Gröschel, C., Brücke, C., Lütjens, G., Schneider, G.-H., Krauss, J.K., Kühn, A.A., Hamker, F.H., 2015. Differential contributions of the globus pallidus and

ventral thalamus to stimulus-response learning in humans. NeuroImage 122, 233–245. doi:10.1016/j.neuroimage.2015.07.061

Schuepbach, W.M.M., Rau, J., Knudsen, K., Volkmann, J., Krack, P., Timmermann, L., Hälbig, T.D., Hesekamp, H., Navarro, S.M., Meier, N., Falk, D., Mehdorn, M., Paschen, S., Maarouf, M., Barbe, M.T., Fink, G.R., Kupsch, A., Gruber, D., Schneider, G.H., Seigneuret, E., Kistner, A., Chaynes, P., Ory-Magne, F., Brefel Courbon, C., Vesper, J., Schnitzler, A., Wojtecki, L., Houeto, J.-L., Bataille, B., Maltête, D., Damier, P., Raoul, S., Sixel-Doering, F., Hellwig, D., Gharabaghi, A., Krüger, R., Pinsker, M.O., Amtage, F., Régis, J.-M., Witjas, T., Thobois, S., Mertens, P., Kloss, M., Hartmann, A., Oertel, W.H., Post, B., Speelman, H., Agid, Y., Schade-Brittinger, C., Deuschl, G., EARLYSTIM Study Group, 2013. Neurostimulation for Parkinson's disease with early motor complications. N Engl J Med 368, 610–622. doi:10.1056/NEJMoa1205158

Setsompop, K., Kimmlingen, R., Eberlein, E., Witzel, T., Cohen-Adad, J., McNab, J.A., Keil, B., Tisdall, M.D., Hoecht, P., Dietz, P., Cauley, S.F., Tountcheva, V., Matschl, V., Lenz, V.H., Heberlein, K., Potthast, A., Thein, H., Van Horn, J., Toga, A., Schmitt, F., Lehne, D., Rosen, B.R., Wedeen, V., Wald, L.L., 2013. Pushing the limits of in vivo diffusion MRI for the Human Connectome Project 80, 220–233. doi:10.1016/j.neuroimage.2013.05.078

Starr, P.A., Turner, R.S., Rau, G., Lindsey, N., Heath, S., Volz, M., Ostrem, J.L., Marks, W.J., Jr., 2006. Microelectrode-guided implantation of deep brain stimulators into the globus pallidus internus for dystonia: techniques, electrode locations, and outcomes. J Neurosurg 104, 488–501. doi:10.3171/jns.2006.104.4.488

Sydow, O., Thobois, S., Alesch, F., Speelman, J.D., 2003. Multicentre European study of thalamic stimulation in essential tremor: a six year follow up., in:. Presented at the

Journal of neurology, neurosurgery, and psychiatry, BMJ Group, pp. 1387–1391. doi:10.1136/jnnp.74.10.1387

Talairach, J., Tournoux, P., 1988. Co-planar Stereotaxic Atlas of the Human Brain. George Thieme Verlag.

Taren, J., Guiot, G., Derome, P., Trigo, J.C., 1968. Hazards of stereotaxic thalamectomy. Added safety factor in corroborating x-ray target localization with neurophysiological methods. J Neurosurg 29, 173–182. doi:10.3171/jns.1968.29.2.0173

Tasker, R.R., Organ, L.W., Hawrylyshyn, P., 1982. Investigation of the Surgical Target for Alleviation of Involuntary Movement Disorders. Stereotact Funct Neurosurg 45, 261–274. doi:10.1159/000101610

Thomas Yeo, B.T., Krienen, F.M., Sepulcre, J., Sabuncu, M.R., Lashkari, D., Hollinshead, M., Roffman, J.L., Smoller, J.W., Zollei, L., Polimeni, J.R., Fischl, B., Liu, H., Buckner, R.L., 2011. The organization of the human cerebral cortex estimated by intrinsic functional connectivity. J Neurophysiol 106, 1125–1165. doi:10.1152/jn.00338.2011

Ughratdar, I., Samuel, M., Ashkan, K., 2015. Technological Advances in Deep Brain Stimulation. J Parkinsons Dis 5, 483–496. doi:10.3233/JPD-150579

Vanegas Arroyave, N., Lauro, P.M., Huang, L., Hallett, M., Horovitz, S.G., Zaghloul, K.A., Lungu, C., 2016. Tractography patterns of subthalamic nucleus deep brain stimulation. Brain aww020. doi:10.1093/brain/aww020

Weiss, K.L., Pan, H., Storrs, J., Strub, W., Weiss, J.L., Jia, L., Eldevik, O.P., 2003. Clinical brain MR imaging prescriptions in Talairach space: technologist- and computer-driven methods. AJNR Am J Neuroradiol 24, 922–929.

Wiesendanger, R., Wiesendanger, M., 1985. Cerebello-cortical linkage in the monkey as revealed by transcellular labeling with the lectin wheat germ agglutinin conjugated to the marker horseradish peroxidase. Experimental brain research Experimentelle Hirnforschung Expérimentation cérébrale 59, 105–117.

Yeh, F.-C., Tseng, W.-Y.I., 2011. NTU-90: a high angular resolution brain atlas constructed by q-space diffeomorphic reconstruction. NeuroImage 58, 91–99. doi:10.1016/j.neuroimage.2011.06.021

Yeh, F.-C., Wedeen, V.J., Tseng, W.-Y.I., 2010. Generalized q-Sampling Imaging. IEEE Trans Med Imaging 29, 1626–1635. doi:10.1109/TMI.2010.2045126

Yelnik, J., Bardinet, E., Dormont, D., Malandain, G., Ourselin, S., Tandé, D., Karachi, C., Ayache, N., Cornu, P., Agid, Y., 2007. A three-dimensional, histological and deformable atlas of the human basal ganglia. I. Atlas construction based on immunohistochemical and MRI data 34, 618–638. doi:10.1016/j.neuroimage.2006.09.026

Zhang, D., Snyder, A.Z., Fox, M.D., Sansbury, M.W., Shimony, J.S., Raichle, M.E., 2008. Intrinsic functional relations between human cerebral cortex and thalamus. J Neurophysiol 100, 1740–1748. doi:10.1152/jn.90463.2008

Supplementary material

Selection of DBS targets based on literature findings (S1)

The PD-DBS cohort used in this study (mean age 59.0 years ± 7.9 SD, 14 female) was retrospectively selected based on a DBS imaging registry of Charité – University Medicine, Berlin. Inclusion criteria were the availability of pre- and postoperative MRI as well as UPDRS-III motor scores available in Med OFF / DBS OFF and Med OFF / DBS ON states. All patients were operated with target STN. 12 of these patients had been enrolled in a double-blinded prospective study targeting the efficacy of STN vs. caudal zona incerta as a DBS target (Schmitz-Hubsch et al., 2014). 16 other patients were enrolled in a study examining the efficacy of DBS in PD with early motor complications (Schuepbach et al., 2013). 11 remaining patients were not enrolled in other imaging studies. Mean Med OFF / Stim OFF UPDRS-III score was 38.7 (±12.8 SD) points. Mean Med OFF / Stim ON score was 18.6 (±8.8 SD), resulting in a relative improvement of 52%.

Selection of DBS targets based on literature findings (S2)

In case of PD, a recent review that averaged reported coordinates of active contacts based on multiple studies in total including 342 electrodes was used (Caire et al., 2013). For dystonia and ET, no similar reviews could be found and results from two highly cited single studies were used (Papavassiliou et al., 2004; Starr et al., 2006). In ET, the original VIM target was defined by Guiot et al (Guiot et al., 1968; Krack et al., 2002). In some studies, this target has been used as a preliminary stereotactic target with the final position refined by microelectrode recordings (Benabid et al., 1996; Taren et al., 1968). In this work, we still focus on the location defined in (Papavassiliou et al., 2004) since it had the largest sample size in comparison to other studies reviewed in a systematic literature search (Atkinson et al., 2002; Benabid et al., 1991; Goldman et al., 1992; Groppa et al.,

2014; Hamel et al., 2007; Mobin et al., 2000; Murata et al., 2003; Pilitsis et al., 2008; Sydow et al., 2003; Tasker et al., 1982), assessed clinical outcome in relation to lead location and is thus more similar in nature to the references used for the other conditions. The Guiot target as defined on a group of subjects in (Krack et al., 2002) is still reported in table 1 alongside with the Papavassiliou target.

Results of these studies were based on 44 and 53 leads. For OCD, based on the review by Höflich et al., the anterior limb of the internal capsule (ALIC), the nucleus accumbens (NAc) and the STN represent main targets (Höflich et al., 2010). No study that included a large cohort of patients could be retrieved in an extensive literature result. Coordinates from a 2-patient case series were used for the NAc (Franzini et al., 2010). In case of the ALIC, the coordinates from the best (and only reported) patient of a study by Nuttin and colleagues (13.5 mm lateral and 3.5 mm anterior to the AC, horizontally on the AC/PC plane – describing the tip of the electrode; Nuttin et al., 2003) and the Talairach coordinates from Anderson et al., (14.5 mm lateral and 8.5 mm anterior to the AC, 8 mm above the AC/PC plane – describing the target coordinate; (D. Anderson and Ahmed, 2003)) were integrated to a mean coordinate (Table 1, Figure 3). Please note that x- and y-coordinates were averaged, z-coordinate was averaged after adding two mm to the coordinate reported by Nuttin (which described the electrode tip). In case of Treatment-Resistant Major Depression (TRD), coordinates from a study by (Hamani et al., 2009) were used. Interestingly, in the seminal paper by Mayberg and colleagues, the target itself was informed by fMRI studies that reported coordinates within MNI space (Hamani et al., 2009; Mayberg et al., 2005). Naturally, in their study, target coordinates were equally calculated within MNI space. A recent meta analysis by (Schrock et al., 2014) assessed availability of coordinates for most studies of DBS in Tourette syndrome (TS). Only 10 of 50 studies reported target coordinates and from this subset, the study with the highest case number was used (Ackermans et al., 2011). Overall, based on a review of (Piedad et

al., 2012), between 1999 and 2012, 99 cases of TS-DBS have been reported and the most promising targets in TS are considered the thalamus and the GPi. For Alzheimer's disease, the mean coordinates from the first publication of the ADvance trial were used (Ponce et al., 2015). In case of addiction, based on a review by Luigjes et al., the most promising target was considered to be the nucleus accumbens (NAc) and coordinates from the first study that used addiction as indication for surgery were used (Luigjes et al., 2011; Müller et al., 2009).

Warping thalamic resources into ICBM 2009b nonlinear space (S3)

Due to slight differences in anatomy provided by MNI templates in various versions (http://nist.mni.mcgill.ca/?page_id=714), some of the MNI resources used here had to be spatially adapted to conform to the newest generation high-res MNI templates used in this study (MNI 152 2009b NLIN asymmetric series). Specifically, popular imaging suites such as SPM12 and FSL5 define standard anatomy using the (older) 6th generation MNI 152 NLIN templates (Grabner et al., 2014) which is only available as a T1 template. Thus, a nonlinear warp from this 6th-generation T1 template to the ICBM 2009b T1 template estimated using ANTs SyN registration (https://dx.doi.org/10.6084/m9.figshare.3502238.v2) had to be applied to the Morel atlas (Jakab et al., 2012) and the Oxford thalamic connectivity atlas (Behrens et al., 2003). The Zhang thalamic connectivity atlas had originally been defined in Washington University 711_2b space. This atlas was equally transformed using a nonlinear warp into 2009b space based on the 711_2b T1 template.

Supplementary figures

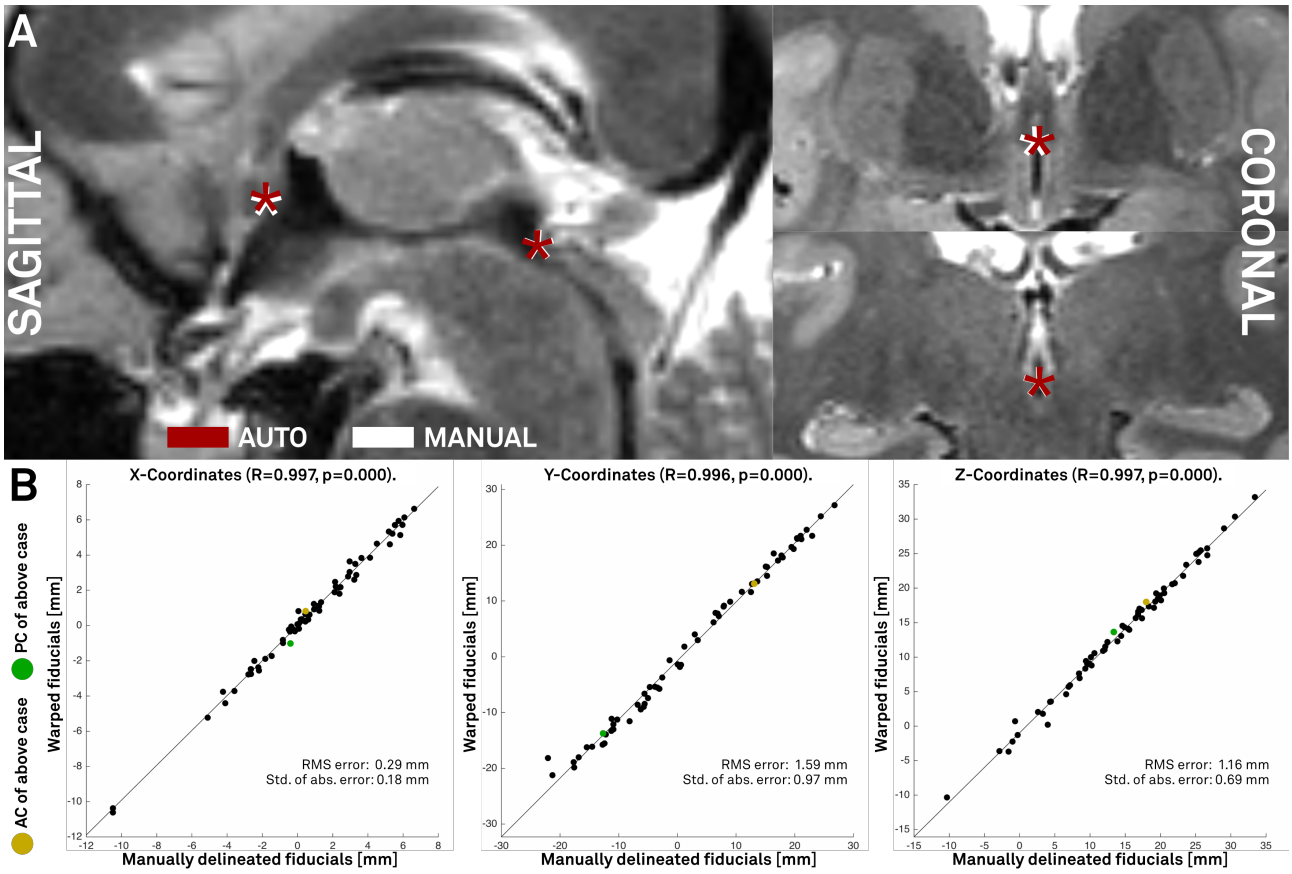

Supplementary Figure S1. Results of automatic AC/PC definition (based on an inverse transform from MNI space) on the Young cohort. A) sagittal and coronal views of a representative subject. Red stars show automatic, white stars manual definitions of AC and PC fiducials, respectively. B) scatter plots of X-, Y- and Z-coordinates of automatic vs. manually defined AC/PC fiducials. AC (yellow) and PC (green) coordinates of the example case demonstrated above are marked in colors.

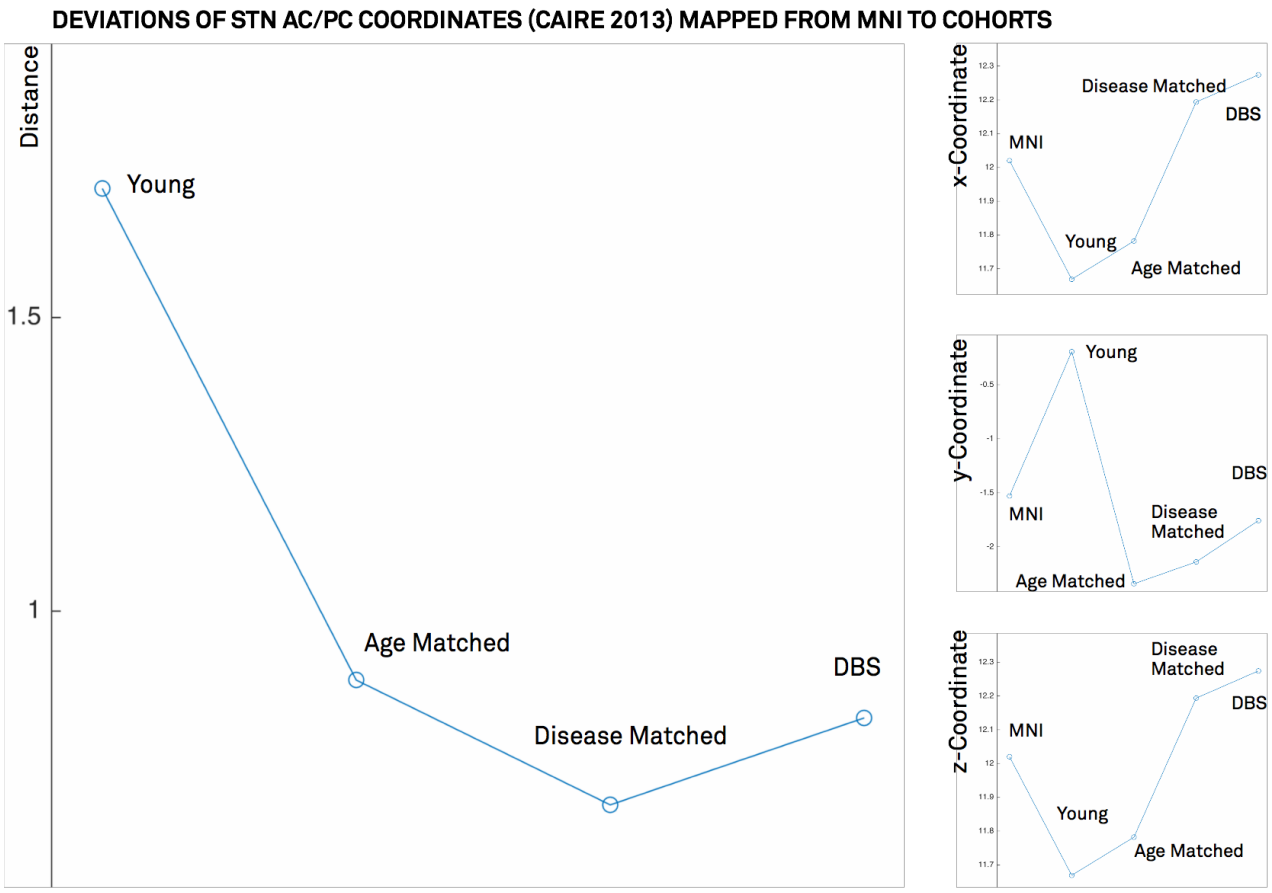

Supplementary Figure S2. Optimal STN-DBS coordinates (Caire 2013) were defined relative to the MCP on the MNI template and warped to all brains of respective coordinates. Average coordinates were then again expressed in the AC/PC-System and compared to the original AC/PC coordinates on the MNI brain (enlarged plot). Distances to coordinates within the Young cohort are higher than for all other cohorts. The small plots on the right show x-, y- and z- AC/PC coordinates within the MNI brain and cohorts. This relationship supports the hypothesis that the reason for an optimal result based on the *MNI survey* method for STN coordinates occurred coincidentally based on the very location of the target. Namely, the STN shifts laterally across the lifespan (Keuken et al., 2013) and thus is located in a similar position in both elderly patients and the (substantially larger) MNI brain.